ADVANCED OPTICAL MATERIALS
www.advopticalmat.de

# Stokes Shift Engineered Mn:CdZnS/ZnS Nanocrystals as Reabsorption-Free Nanoscintillators in High Loading Polymer Composites

*Francesco Carulli, Francesca Cova, Luca Gironi, Francesco Meinardi, Anna Vedda, and Sergio Brovelli**

**Plastic scintillators are gaining attention as alternatives to inorganic scintillator crystals owing to their low fabrication cost, customable shape/size, and substantially lighter weight that make them suitable for various radiation detection technologies. These include scintillation panels for national security and industrial monitoring, radiation screens for medical diagnostics, and calorimeters for high energy physics. Because of their low density, plastic scintillators are typically doped with high atomic number (*Z*) sensitizers that enhance the interaction probability with ionizing radiation and excite molecular emitters. Although effective, such a two-component design suffers from incomplete sensitization, intrinsically limited efficiency due to multiple radiative steps with non-unity quantum yield, detrimental phase segregation effects and the fragility of organic emitters to ionizing radiation. In this work, an alternative single-component scheme is proposed based on high-*Z* reabsorption-free CdZnS/ZnS semiconductor nanocrystals (NCs) doped with manganese embedded in a polyvinyltoluene (PVT) waveguide. Optical-grade nanocomposites free from optical reabsorption of the scintillation light and with performance comparable to commercial products are obtained through a post-synthesis resurfacing procedure that maximizes the compatibility between the NCs and PVT and preserves their optical properties upon curing.**

## 1. Introduction

Efficient detection of ionizing radiation plays a central role in several scientific and technological fields such as high energy and particle physics, astronomy, geology, medical diagnostics, nuclear monitoring, oil extraction, and space exploration.[1] In all such areas the most widely used detectors are scintillating materials that convert the energy deposited by incoming ionizing radiation into visible photons, which are then turned into electrical signals by coupled photodetectors (e.g. photomultiplier tubes or silicon photomultipliers).[2] The relatively simple device architecture and the availability of high atomic number (*Z*) materials efficiently interacting with ionizing radiation of various energies (the interaction probability scales with $Z^n$ with $n = 1–5$ depending on the interaction mechanism[1f,3]) is enabling rapid progress in the design of scintillators optimized for specific application requirements.[4] A valuable class of radiation detectors is represented by plastic scintillators that can be produced in large sizes not achievable with inorganic single crystals, low weight, and affordable costs that make them particularly suitable for radiation monitoring in border and industrial control.[2b,5] However, being constituted of light organic materials, plastic scintillators typically suffer from relatively low density that limits their interaction with ionizing radiation and therefore require doping with high-*Z* components, such as organometallic complexes or nanoparticles containing heavy elements.[2b,6] Amongst the various systems proposed to date, direct bandgap colloidal semiconductor nanocrystals (NCs) featuring efficient excitonic photophysics, such as cadmium or zinc chalcogenides or lead halide perovskites, are gaining particular interest as nanoscintillators, as they both enhance the interaction probability with ionizing radiation and effectively convert the deposited energy into visible light whose wavelength can be finely tuned by size and composition control.[2b,7] Furthermore, NCs also feature a rich surface chemistry[8] that enables their post-synthesis functionalization with molecular ligands that prompt their compatibility with plastic matrices, thus enabling the realization of

F. Carulli, F. Cova, F. Meinardi, A. Vedda, S. Brovelli
Dipartimento di Scienza dei Materiali
Università degli Studi di Milano-Bicocca
Milano 20125, Italy
E-mail: sergio.brovelli@unimib.it
F. Cova, L. Gironi, A. Vedda, S. Brovelli
INFN Sezione Milano – Bicocca
Piazza della Scienza 3, Milano I-20126, Italy
L. Gironi
Dipartimento di Fisica
Università degli Studi di Milano-Bicocca
Milano 20125, Italy
The ORCID identification number(s) for the author(s) of this article can be found under https://doi.org/10.1002/adom.202200419.



**DOI: 10.1002/adom.202200419**

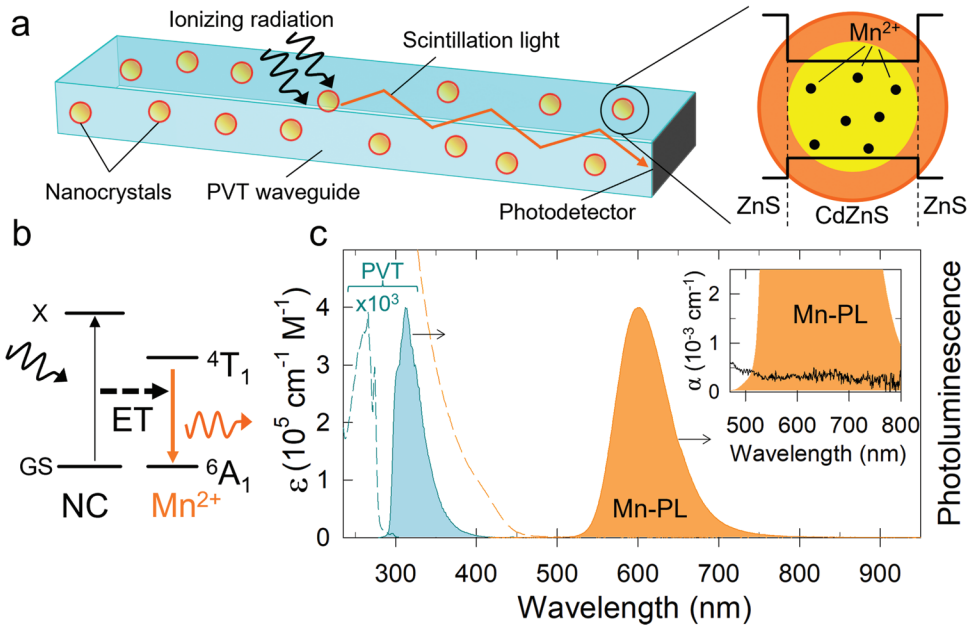


**Figure 1.** a) On the left: Schematic representation of a nanocomposite scintillator incorporating Mn:CdZnS/ZnS NCs. Incident ionizing radiation (black arrows) interacts with the PVT/NCs nanocomposite resulting in the emission of visible photons (orange arrows) guided via total internal reflection to the waveguide edges. On the right: simplified structure of the band alignment of Mn:CdZnS/ZnS core/shell NC. b) Scheme of the recombination process in Mn:CdZnS/ZnS NCs showing sensitization of the $^4T_1 \rightarrow {}^6A_1$ to $Mn^{2+}$ dopants by host excitons produced upon interaction with ionizing radiation. c) Optical absorption (dashed lines) and PL spectra (continuous lines) of PVT (blue lines) and Mn:CdZnS/ZnS NCs (orange lines). Inset: Magnification of the spectral region corresponding to the Mn-PL (for a 1 mM NC solution in $CHCl_3$) showing negligible absorption coefficient (black line).

high optical quality nanocomposites with relatively large NCs weight fraction.[6b,9] However, because of the characteristic small Stokes shift of direct bandgap materials leading to a large spectral overlap between their absorption and luminescence spectra, one common issue with using NCs as nanoscintillators in highly dense or large volume detectors is represented by the strong reabsorption of the scintillation light along its path to the perimetral photodetectors. The typical strategy adopted to circumvent such a reabsorption bottleneck is a hybrid design where NCs act as high-*Z* sensitizers for secondary organic emitters featuring a large Stokes shift typically prompted by molecular planarization in the excited state.[2b,9b] However, this approach suffers some intrinsic limitations represented by the high concentration of molecular emitters required for efficiently transferring excitation from the NCs via energy transfer that may result in phase segregation and molecular aggregation, and by the incomplete spectral separation between the optical absorption luminescence profiles of organic dyes, ultimately resulting in substantial residual reabsorption losses in very large detectors and in the intrinsic fragility of conjugated organic emitters exposed to prolonged ionizing radiation.

For these reasons, realizing nanocomposite scintillators in which NCs with specifically engineered large Stokes shift act as both efficient radiation harvesters and reabsorption-free emitters would strongly benefit the field and offer a valuable alternative to existing hybrid technologies. Recently, various examples of this design have been provided by exploiting self-trapped excitons in metal halides.[10] In this work, we aim at contributing to this endeavor by realizing new plastic scintillators consisting in a polyvinyltoluene (PVT) matrix incorporating reabsorption-free CdZnS/ZnS core/shell NCs doped with manganese ions (hereafter referred to as Mn:CdZnS/ZnS, **Figure 1**a). Manganese doping of large bandgap NCs is an established approach to activate efficient luminescence at ≈580–600 nm arising from the $^4T_1 \rightarrow {}^6A_1$ optical transition on $Mn^{2+}$ color centers[11] (Figure 1b). Representative optical absorption and photoluminescence (PL) spectra of our NCs are shown in Figure 1c. Crucially, since such a transition is spin-forbidden, the corresponding optical absorption features negligible oscillation strength (see inset of Figure 1c), resulting in an apparent Stokes shift between the band-edge absorption of the host NC and the Mn-PL. As a result, Mn-doped NCs have been successfully implemented as reabsorption-free emitters in luminescent solar concentrators (LSC)[11d,12] which, similar to plastic scintillators, convert impinging radiation (sunlight in the case of LSC) into visible luminescence trapped into total internal reflection propagation modes of a doped optical waveguide and collect it using efficient photodetectors placed along the slab edges.[13] In our approach to reabsorption-free nanoscintillators, we further adopted a synergic strategy in which both the PVT waveguide and the NCs interact with incoming ionizing radiation, while the propagating luminescence is generated by the sole NCs, whose optical properties are specifically engineered to absorb the PVT emission (reported in blue in Figure 1c). The emission efficiency and compatibility of the NCs with the polymer host were optimized by combining inorganic shelling in type-I configuration using wide bandgap ZnS overgrown on top of the Mn:CdZnS cores and surface functionalization with crosslinking ligands that participate in the radical polymerization of the PVT waveguide. Overall, this design results in high optical quality nanocomposites nearly perfectly transparent in the spectral region of their own emission, with scintillation efficiency comparable to commercial plastic scintillators.

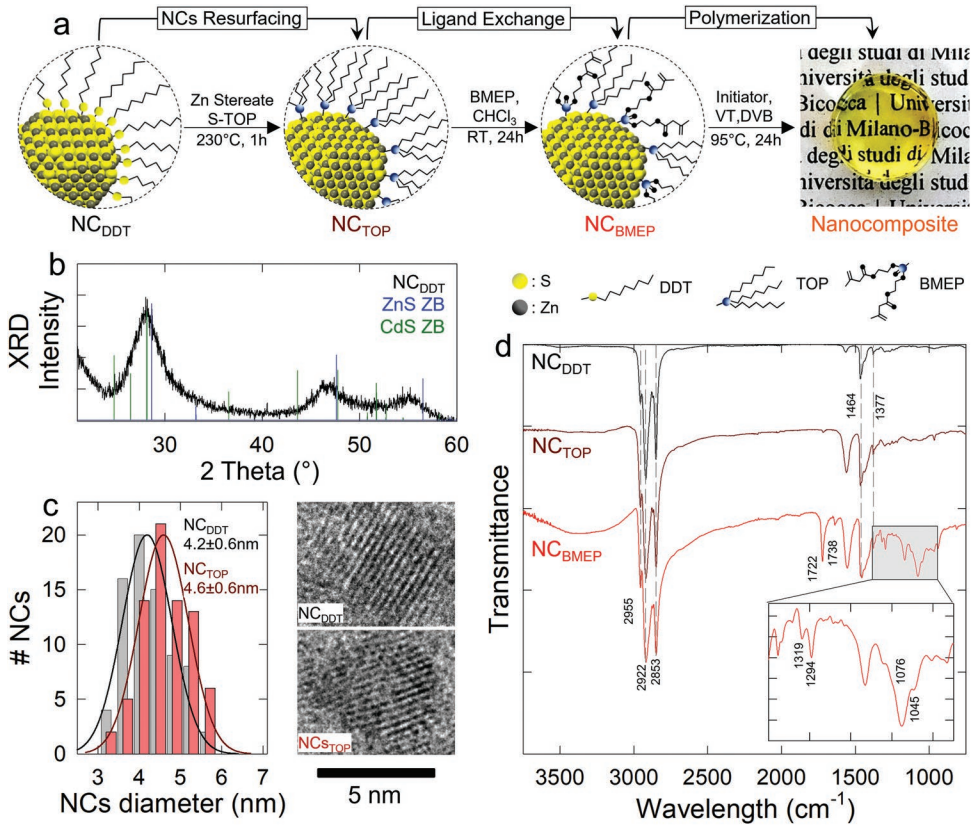


**Figure 2.** a) Schematics of the three-step procedure adopted for the synthesis, resurfacing, and embedding of Mn:$Cd_{0.5}Zn_{0.5}S$/ZnS NCs into PVT. DDT-, BMEP-, and TOP-capped NCs are here indicated as $NC_{DDT}$, $NC_{BMEP}$, and $NC_{TOP}$, respectively. The final panel shows a picture of a nanocomposite embedding $NC_{TOP}$ (1 wt%). b) XRD pattern of $NC_{DDT}$ compared to bulk ZnS (blue line—ICSD 53943) and CdS (green line—ICSD 31074) in zincblende crystal structure. c) TEM images of $NC_{DDT}$ and $NC_{TOP}$ together with the respective size distribution. d) FTIR spectra of $NC_{DDT}$, $NC_{TOP}$, and $NC_{BMEP}$ samples. IR absorption bands at 2955 $cm^{-1}$ ($CH_3$ bending), 2922 $cm^{-1}$, 2853 $cm^{-1}$ ($CH_2$ stretching), 1464 $cm^{-1}$ ($CH_2$ scissoring), and 1377 $cm^{-1}$ ($CH_2$ bending) are ascribed to the long aliphatic chains of DDT and TOP ligands. The absorption features of $NC_{BMEP}$ sample at 1722, 1738 $cm^{-1}$ (C=O and C=C vibrational modes), and in the 1400–950 $cm^{-1}$ spectral region are ascribed to BMEP acrylic and phosphonate groups, respectively (1319, 1294 $cm^{-1}$ P=O stretching, 1076, 1045 $cm^{-1}$ P—O—C stretching).

## 2. Results and Discussion

Mn:CdZnS/ZnS NCs optimized for integration into high optical quality polymeric waveguides were produced following the multi-step strategy schematized in **Figure 2**a. As a first step, core/shell Mn:CdZnS/ZnS NCs (5% Mn doping in respect Cd and Zn content) were synthetized through a non-injection synthesis[14] where CdZnS cores are grown by heating the precursors in the presence of a manganese source. In our case, we adopted hexadecane as reaction solvent instead of 1-octadecene used in ref, [14], as it ensures a better optical quality of the NCs for further incorporation in the polymeric matrix. ZnS shelling was performed through a layer-by-layer deposition by continuous injection of shell precursor at 230 °C (see Methods section in Supporting Information for details).[14,15] Consistent with previous results,[14] the obtained NCs are in a zincblende crystal structure (as shown by the X-ray diffraction pattern in Figure 2b) and feature a mean diameter <*d*> of 4.2 nm (Figure 2c). It is important to underline that in this synthetic way the excess of dodecane thiol (DDT) is used both as a source of sulfur (together with the elemental S) and as a capping ligand, which allows to obtain a PL with a high quantum efficiency (PLQY). However, DDT-capped NCs exhibit poor solubility in the vinyl toluene monomer solution used for fabrication of the nanocomposite scintillator resulting in noticeable light scattering even at very low NCs concentrations (Figure S1, Supporting Information). In order to overcome this limitation, we thus performed a two-step resurfacing procedure to replace DDT ligands, which are strongly bound to the NC's surface, with bis[2-(methacryloyloxy)ethyl] phosphate (BMEP) whose terminal acrylic functionalities participate in the polymerization process and thus lead to homogeneous transparent nanocomposites even at high NCs loadings. With this aim we first grew an additional ZnS layer on top of DDT-capped NCs using an excess of trioctylphosphine (TOP) capping ligands. Such an intermediate step is pivotal since it greatly facilitates the subsequent ligand exchange process, as TOP can be easily substituted by BMEP due to its electronically neutral configuration in both attached and desorbed form. On the contrary, direct replacement of DDT ligand is challenging due to the very low electrostatic stabilization of electronically charged DDT moieties detached from the particle surface, resulting in energetically unfavorable dissociation.[8] Consistently, our efforts to directly exchange DDT to BMEP have yielded no results.

Specifically, TOP resurfacing was performed as a one-pot procedure by adding Zn stearate and tri-octyl-phosphine sulfide (TOP-S) to the DDT-capped NCs. The deposition of the TOP-capped ZnS layer was verified by comparing the average size distribution of the NCs from TEM images collected before and after resurfacing. As shown in Figure 2c, TOP-capped NCs feature $<d> = 4.6 \pm 0.6$ nm, which is 0.4 nm larger than DDT-capped NCs corresponding to approximately one monolayer of ZnS.[14,16] As a second step, TOP ligands were exchanged with BMEP, as confirmed by Fourier transform infrared (FTIR) spectroscopy measurements reported in Figure 2d, showing the characteristic peaks of the P=O, P−OR bonds of BMEP in the 1000–1400 $cm^{-1}$ range.[6b,9a]

Finally, nanocomposite samples were produced via thermally activated polymerization of vinyl toluene (VT) loaded with BMEP-capped NCs. To do so, BMEP-capped NCs were washed three times from unreacted BMEP ligands by addition of excess acetone and precipitated and dried with $N_2$. Subsequently, NCs were dissolved in VT (containing 5% V/V of divinylbenzene as crosslinker) and sonicated until a clear solution was obtained. The polymerization was then performed by heating the VT/NCs solution in a mold following an optimized thermal ramp for avoiding contraction effects and the formation of defects in the nanocomposite surfaces. After 24 h, the mold was let to cool down to room temperature and the nanocomposite was extracted, cut, and polished for further spectroscopic studies. The right panel of Figure 2a shows the photograph of a PVT/NCs nanocomposite under ambient light. As it will be quantified below, the nanocomposites exhibit high optical quality and negligible haze due to NCs agglomeration or structural defects, which corroborates the effectiveness of the compatibilization strategy.

Crucially, the optical properties of the NCs are perfectly preserved at all steps of the surface functionalization process, as well as after embedding into the PVT matrix. The optical absorption and PL spectra of DDT-, TOP-, and BMEP-capped NCs and of the nanocomposite sample are reported in **Figure 3**a showing identical profiles with the absorption edge at 420 nm and a broad Stokes-shifted PL at 595 nm. All samples also exhibit comparable slightly multiexponential PL dynamics with effective lifetime (measured as the time after which the PL intensity has dropped by a factor *e*) of 0.9 ms (Figure 3b). Possibly more importantly, the PL efficiency is identical for all NCs samples within the experimental uncertainty (PLQY ≈ 65 ± 6%) and only slightly lower in the nanocomposite (PLQY = 55 ± 7%), as shown in the inset of Figure 3b. Crucially, the radioluminescence (RL) spectrum of the nanocomposite, shown as a shaded curve in Figure 3a, is identical to the corresponding PL, indicating that the scintillation process leads to the same recombination mechanism as UV illumination and that no defects related radiative emissions emerge under ionizing radiation. Based on the promising properties of the Mn:CdZnS/ZnS NCs, we proceeded with investigating the scintillation process in PVT/NCs nanocomposites via RL experiments as a function of the NCs loading in PVT matrices (from 0 to 8 wt%, as measured via thermo gravimetric analysis shown in Figure S2, Supporting Information). Consistent with the typical scintillation behavior of PVT, the bare matrix shows the characteristic RL spectrum centered at 320 nm (Figure 3c). Upon increasing the NCs loading leads to the progressive decrease of the PVT-RL, which is accompanied by the raise of the NCs emission, as quantified in Figure 3e, where we report the integrated intensity of the total RL together with the individual contribution by the PVT and the NCs. This is consistent with the complete match between the PVT emission and the NCs absorption. Time-resolved measurements of the PVT luminescence on the same samples (Figure 3d) reveal that the drop of the PVT-RL with increasing NCs content is accompanied by a very minor acceleration of the PVT emission kinetics (from effective $\tau = 5.8$ ns of bare PVT to $\tau = 5.2$ ns for [NC] = 1 wt%), which indicates that the dominant optical process is the absorption of the PVT-RL by the NCs followed by re-emission, whereas non-radiative energy transfer plays a negligible role (see Supporting Information for detailed analysis). A closer look at the integrated RL intensities in Figure 3e further reveals that for NCs contents above 0.2 wt% the total RL emitted by the nanocomposite is dominated by the NCs-RL, whereas the PVT contribution is quenched by over 95%. For lower NCs loadings, on the other hand, the interaction with X-rays occurs mostly with PVT, resulting in PVT-dominated RL. Because of the non-unitary PLQY of the NCs, at intermediate concentrations when the RL is also largely due to indirect NCs excitation by PVT, the total scintillation signal drops with respect to the bare PVT matrix. In order to provide a figure of merit of the scintillation performance of our proof-of-concept nanocomposites, we compared their RL with that of a commercial plastic scintillator (EJ-276 from Eljen Technology) measured in the same experimental conditions. The nanocomposite containing 8 wt% of NCs showed a RL signal comparable to EJ-276 (with reported light yield of 8600 Ph $MeV^{-1}$), corresponding to a relative light yield of 5900 ± 600 Ph $MeV^{-1}$ (see Figure S4, Supporting Information). Finally, we tested the stability of the RL performance under continuous X-ray irradiation (Figure 3g) up to total absorbed dose of 20 Gy. The RL intensity preserved over 95% of its initial value, independently from the concentration of embedded NCs. The RL spectrum shows no modification upon prolonged X-ray exposure, suggesting that our NCs are suitable also for continuous radiation detection.

Finally, we experimentally validated our approach to reabsorption-free plastic scintillators using doped NCs by fabricating a 20 cm long PVT scintillator waveguide containing 0.2 wt% of NCs and characterizing its light guiding properties under X-ray irradiation. To do so, we collected the RL spectra as a function of the distance, *d*, between the X-ray excitation beam and the device edge as schematized in **Figure 4**a. The RL spectra collected at increasing *d* are reported in Figure 4b and show identical spectral profile and intensity, which confirms that the scintillator is completely unaffected by reabsorption effects. Consistently, as quantified in Figure 4c, the integrated RL intensity is constant for all *d*-values within the experimental uncertainty, which also confirms that our nanocomposite scintillator waveguide is unaffected by light scattering losses, thus further corroborating the high optical quality of the nanocomposite and the effectiveness of the NCs surface functionalization. The same results are obtained using optical excitation with 3.05 eV light. Also in this case, increasing *d* does not influence the PL spectrum profile (reported in Figure S5, Supporting Information) or the PL output intensity.

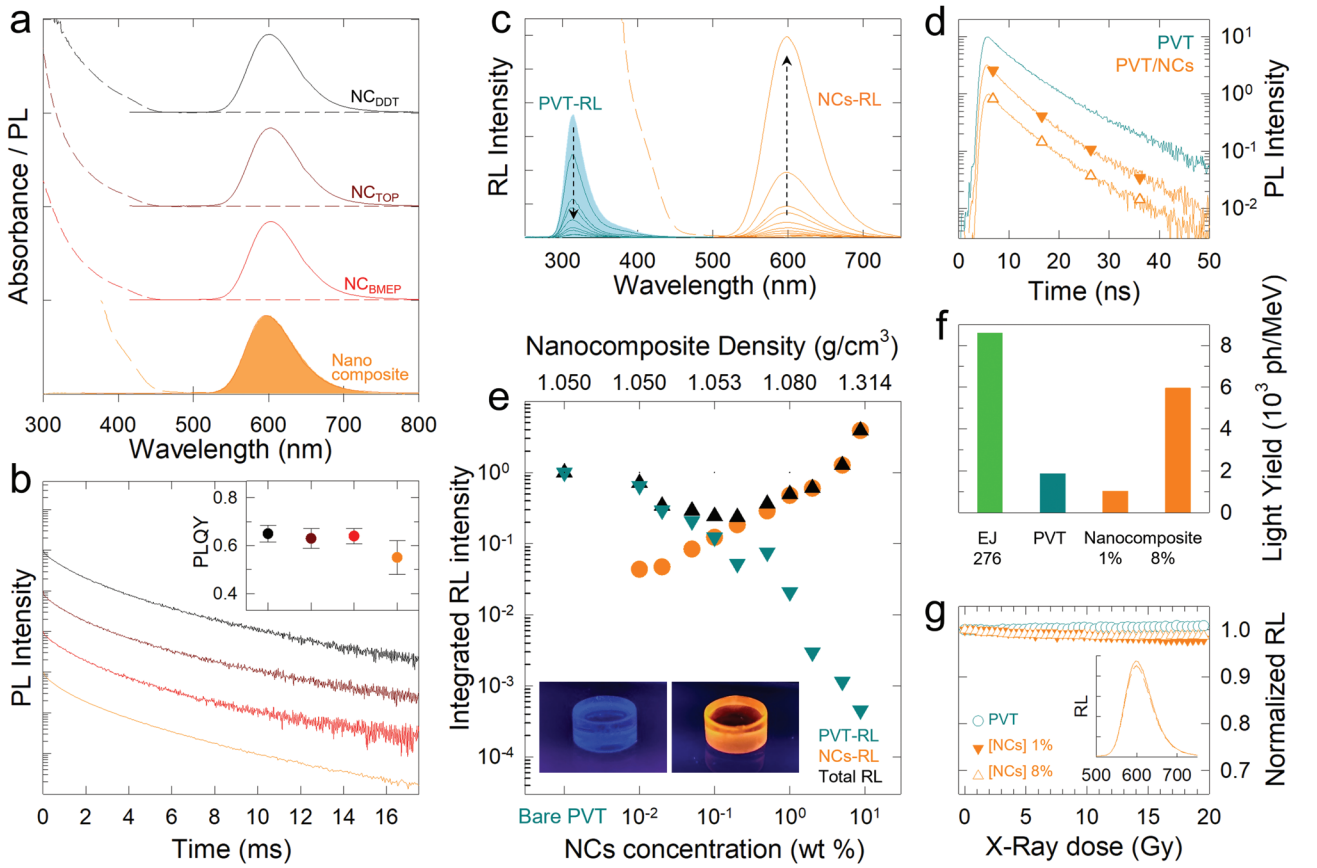


**Figure 3.** a) Absorption (dashed lines) and PL (continuous lines) spectra of NCs at different processing steps in toluene solutions and in the nanocomposite. DDT-, BMEP-, and TOP-capped NCs are here indicated as $NC_{DDT}$, $NC_{BMEP}$, and $NC_{TOP}$, respectively. The shaded spectrum refers to RL of a nanocomposite with 1 wt% of NCs. b) PL decay traces of NCs samples in toluene during surface functionalization and in the nanocomposite. In the inset the PLQY of NCs in toluene solutions during processing and in the final nanocomposite are reported. The color scheme is the same adopted in plot a. c) RL spectra of a set of PVT/NCs nanocomposites with increasing amount of NCs (from 0 to 10 wt%, indicated by the arrows) excited with soft X-rays. Emissions of PVT and of NCs are blue and orange, respectively. Nanocomposite (1 wt% NCs) absorption spectrum is reported as a dashed line. d) Decay traces of PVT emission (collection wavelength 320 nm) under 254 nm excitation in bare PVT sample (blue curve) and in nanocomposite with 1 wt% (filled triangles) and 8 wt% (hollow triangles) of NCs. e) Integrated RL intensity extracted from the spectra in (c) as a function of the NCs concentration. The contributions from PVT, NCs, and total emission are reported as blue, orange, and black symbols, respectively. Inset: photographs of a PVT sample (left) and of a PVT/NC nanocomposite (1 wt% of NCs, right) under UV illumination at 254 nm. The density of the nanocomposites was evaluated as the average density of the polymer host and the NC loading considering the respective weight fractions. f) Light yield of a commercial plastic scintillator (EJ-276) used as reference, of bare PVT and of nanocomposite samples with different NCs loading. g) Normalized integrated RL intensity of samples of PVT, and nanocomposites as a function of continuous X-ray irradiation. Inset: RL spectra collected before (0 Gy) and after (20 Gy) exposure, showing no variation of the RL profile.

## 3. Conclusion

In summary, we have realized a reabsorption-free nanocomposite plastic scintillator based on a PVT matrix loaded with Mn-doped core/shell CdZnS/ZnS NCs. Post-synthesis engineering of the NCs surfaces enabled us to preserve the optical features of the NCs after the thermally activated radical polymerization of the polymeric matrix. Optical and scintillation investigations as a function of the NCs loading highlighted that our PVT-NCs composite scintillators exploit the scintillating properties of both the NCs and the plastic waveguide and exhibit performance comparable to optimized commercial plastic scintillators. Finally, we experimentally validated the effective suppression of reabsorption losses on the radioluminescence by monitoring the waveguiding performance of a large-size NC-based device under X-ray excitation, confirming that our strategy can be successfully implemented also in large-scale plastic scintillators.

## Supporting Information

Supporting Information is available from the Wiley Online Library or from the author.

## Acknowledgements

This work was supported by the Italian Ministry of University and Research (MIUR) through grant Dipartimenti di Eccellenza—2017 "Materials for Energy." This project has received funding from the

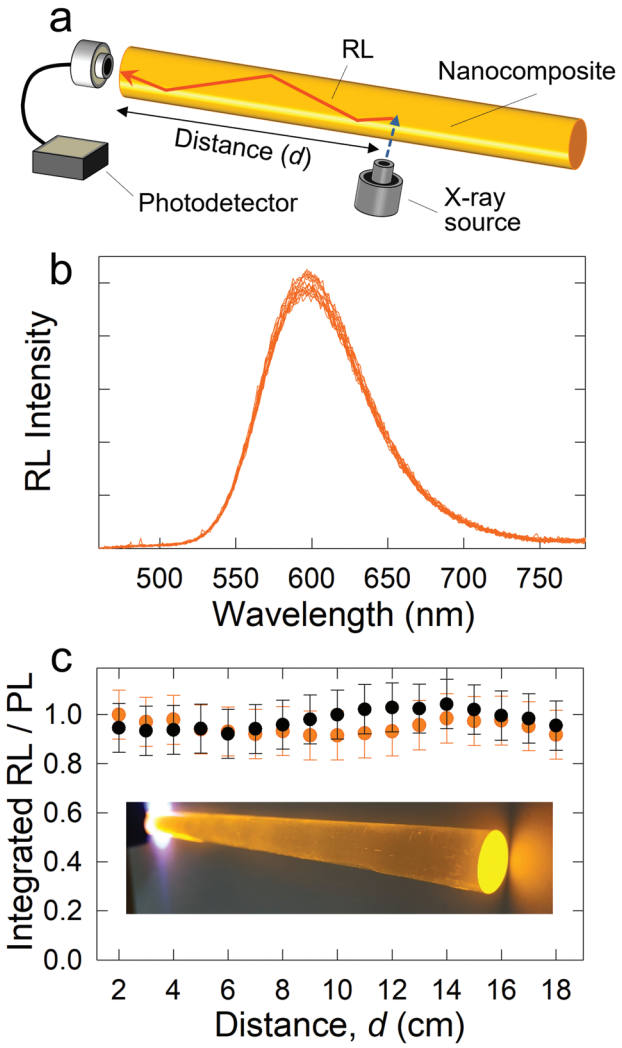


**Figure 4.** a) Sketch of the experimental configuration used for the RL propagation measurements. b) RL spectra collected at increasing distance, *d*, from the nanocomposite edge. Spectra collected from the outer portion of nanocomposite (from 0 to 2 and from 18 to 20 cm) have been omitted to avoid erroneous evaluation of the RL intensity due to the different geometrical collection factor. The sample was excited by X-ray beam of 10 mm diameter. c) Integrated RL (orange dots) and PL (black dots) intensities as a function of *d* extracted from the RL spectra in (b) and the PL spectra in Figure S5, Supporting Information.

European Union's Horizon 2020 Research and Innovation programme under Grant Agreement No 101004761.

Open Access Funding provided by Universita degli Studi di Milano-Bicocca within the CRUI-CARE Agreement.

## Conflict of Interest

The authors declare no conflict of interest.

## Data Availability Statement

The data that support the findings of this study are available from the corresponding author upon reasonable request.

## Keywords

doping, nanocrystals, polivinyltoluene, reabsorption-free, scintillators

Received: February 22, 2022
Revised: March 21, 2022
Published online:

[1] a) B. D. Milbrath, A. J. Peurrung, M. Bliss, W. J. Weber, *J. Mater. Res.* **2008**, *23*, 2561; b) C. W. E. v. Eijk, *Phys. Med. Biol.* **2002**, *47*, R85; c) M. L. McConnell, P. F. Bloser, J. Legere, J. M. Ryan, *J. Phys.: Conf. Ser.* **2016**, *763*, 012008; d) J. H. Baker, N. Z. Galunov, A. M. Stepanenko, O. A. Tarasenko, *Radiat. Meas.* **2004**, *38*, 817; e) J. H. Baker, N. Z. Galunov, O. A. Tarasenko, presented at 2007 IEEE Nuclear Science Symp. Conf. Record, IEEE Operations Center, Piscataway, NJ October **2007**; f) G. F. Knoll, *Radiation detection and measurement*, John Wiley & Sons, Hoboken, NJ **2010**; g) C. Kim, W. Lee, A. Melis, A. Elmughrabi, K. Lee, C. Park, J.-Y. Yeom, *Crystals* **2021**, *11*, 669; h) M. Hoheisel, *Nucl. Instrum. Methods Phys. Res., Sect. A* **2006**, *563*, 215; i) Y. Eisen, A. Shor, I. Mardor, *Nucl. Instrum. Methods Phys. Res., Sect. A* **1999**, *428*, 158; j) R. Carchon, M. Moeslinger, L. Bourva, C. Bass, M. Zendel, *Nucl. Instrum. Methods Phys. Res., Sect. A* **2007**, *579*, 380; k) G. Zentai, *Int. J. Signal Imaging Syst. Eng.* **2010**, *3*, 13; l) P. J. Sellin, *Nucl. Instrum. Methods Phys. Res., Sect. A* **2003**, *513*, 332; m) E. Fredenberg, *Nucl. Instrum. Methods Phys. Res., Sect. A* **2018**, *878*, 74.

[2] a) P. Lecoq, A. Gektin, M. Korzhik, *Inorganic Scintillators for Detector Systems*, Springer, London **2006**; b) M. Gandini, I. Villa, M. Beretta, C. Gotti, M. Imran, F. Carulli, E. Fantuzzi, M. Sassi, M. Zaffalon, C. Brofferio, L. Manna, L. Beverina, A. Vedda, M. Fasoli, L. Gironi, S. Brovelli, *Nat. Nanotechnol.* **2020**, *15*, 462.

[3] G. R. Gilmore, in *Practical Gamma-Ray Spectrometry*, John Wiley & Sons, Hoboken, NJ **2008**.

[4] a) C. Dujardin, E. Auffray, E. Bourret-Courchesne, P. Dorenbos, P. Lecoq, M. Nikl, A. N. Vasil'ev, A. Yoshikawa, R. Y. Zhu, *IEEE Trans. Nucl. Sci.* **2018**, *65*, 1977; b) P. Lecoq, *IEEE Trans. Radiat. Plasma Med. Sci.* **2017**, *1*, 473; c) M. Zhang, X. Wang, B. Yang, J. Zhu, G. Niu, H. Wu, L. Yin, X. Du, M. Niu, Y. Ge, Q. Xie, Y. Yan, J. Tang, *Adv. Funct. Mater.* **2021**, *31*, 2007921.

[5] J. Glodo, Y. Wang, R. Shawgo, C. Brecher, R. H. Hawrami, J. Tower, K. S. Shah, *Phys. Procedia* **2017**, *90*, 285.

[6] a) B. L. Rupert, N. J. Cherepy, B. W. Sturm, R. D. Sanner, S. A. Payne, *Europhys. Lett.* **2012**, *97*, 22002; b) C. Liu, Z. Li, T. J. Hajagos, D. Kishpaugh, D. Y. Chen, Q. Pei, *ACS Nano* **2017**, *11*, 6422; c) J. Perego, I. Villa, A. Pedrini, E. C. Padovani, R. Crapanzano, A. Vedda, C. Dujardin, C. X. Bezuidenhout, S. Bracco, P. E. Sozzani, A. Comotti, L. Gironi, M. Beretta, M. Salomoni, N. Kratochwil, S. Gundacker, E. Auffray, F. Meinardi, A. Monguzzi, *Nat. Photonics* **2021**, *15*, 393; d) Q. Chen, J. Wu, X. Ou, B. Huang, J. Almutlaq, A. A. Zhumekenov, X. Guan, S. Han, L. Liang, Z. Yi, J. Li, X. Xie, Y. Wang, Y. Li, D. Fan, D. B. L. Teh, A. H. All, O. F. Mohammed, O. M. Bakr, T. Wu, M. Bettinelli, H. Yang, W. Huang, X. Liu, *Nature* **2018**, *561*, 88.

[7] a) K. M. McCall, K. Sakhatskyi, E. Lehmann, B. Walfort, A. S. Losko, F. Montanarella, M. I. Bodnarchuk, F. Krieg, Y. Kelestemur, D. Mannes, Y. Shynkarenko, S. Yakunin, M. V. Kovalenko, *ACS Nano* **2020**, *14*, 14686; b) H. Zhang, Z. Yang, M. Zhou, L. Zhao, T. Jiang, H. Yang, X. Yu, J. Qiu, Y. Yang, X. Xu, *Adv. Mater.* **2021**, *33*, 2102529; c) Z. Kang, Y. Zhang, H. Menkara, B. K. Wagner, C. J. Summers, W. Lawrence, V. Nagarkar, *Appl. Phys. Lett.* **2011**, *98*, 181914; d) Z. Fang, H. Tang, Z. Yang, H. Zhang, Q. Peng, X. Yu, D. Zhou, J. Qiu, X. Xu, *Adv. Opt. Mater.* **2021**, *9*, 2101607; e) Y. Liu, M. S. Molokeev, Z. Xia, *Energy Mater. Adv.* **2021**, *2021*, 2585274;

f) H. Yang, L. Gutiérrez-Arzaluz, P. Maity, M. A. Abdulhamid, J. Yin, Y. Zhou, C. Chen, Y. Han, G. Szekely, O. M. Bakr, O. F. Mohammed, *Energy Mater. Adv.* **2021**, *2021*, 9873846; g) F. Zhang, Z. Ma, Z. Shi, X. Chen, D. Wu, X. Li, C. Shan, *Energy Mater. Adv.* **2021**, *2021*, 5198145; h) L. Lian, M. Zheng, W. Zhang, L. Yin, X. Du, P. Zhang, X. Zhang, J. Gao, D. Zhang, L. Gao, G. Niu, H. Song, R. Chen, X. Lan, J. Tang, J. Zhang, *Adv. Sci.* **2020**, *7*, 2000195.

[8] M. A. Boles, D. Ling, T. Hyeon, D. V. Talapin, *Nat. Mater.* **2016**, *15*, 141.

[9] a) Y. Jin, D. Kishpaugh, C. Liu, T. J. Hajagos, Q. Chen, L. Li, Y. Chen, Q. Pei, *J. Mater. Chem. C* **2016**, *4*, 3654; b) C. Liu, T. J. Hajagos, D. Kishpaugh, Y. Jin, W. Hu, Q. Chen, Q. Pei, *Adv. Funct. Mater.* **2015**, *25*, 4607.

[10] a) D. Zhu, M. L. Zaffalon, V. Pinchetti, R. Brescia, F. Moro, M. Fasoli, M. Fanciulli, A. Tang, I. Infante, L. De Trizio, S. Brovelli, L. Manna, *Chem. Mater.* **2020**, *32*, 5897; b) V. Morad, Y. Shynkarenko, S. Yakunin, A. Brumberg, R. D. Schaller, M. V. Kovalenko, *J. Am. Chem. Soc.* **2019**, *141*, 9764; c) W. Gao, G. Niu, L. Yin, B. Yang, J.-H. Yuan, D. Zhang, K.-H. Xue, X. Miao, Q. Hu, X. Du, J. Tang, *ACS Appl. Electron. Mater.* **2020**, *2*, 2242; d) D. Zhu, M. L. Zaffalon, J. Zito, F. Cova, F. Meinardi, L. De Trizio, I. Infante, S. Brovelli, L. Manna, *ACS Energy Lett.* **2021**, *6*, 2283; e) K. M. McCall, V. Morad, B. M. Benin, M. V. Kovalenko, *ACS Mater. Lett.* **2020**, *2*, 1218.

[11] a) S. Sapra, A. Prakash, A. Ghangrekar, N. Periasamy, D. D. Sarma, *J. Phys. Chem. B* **2005**, *109*, 1663; b) D. J. Norris, N. Yao, F. T. Charnock, T. A. Kennedy, *Nano Lett.* **2001**, *1*, 3; c) N. Pradhan, *J. Phys. Chem. Lett.* **2019**, *10*, 2574; d) F. Meinardi, Q. A. Akkerman, F. Bruni, S. Park, M. Mauri, Z. Dang, L. Manna, S. Brovelli, *ACS Energy Lett.* **2017**, *2*, 2368; e) X. Yang, C. Pu, H. Qin, S. Liu, Z. Xu, X. Peng, *J. Am. Chem. Soc.* **2019**, *141*, 2288.

[12] C. S. Erickson, L. R. Bradshaw, S. McDowall, J. D. Gilbertson, D. R. Gamelin, D. L. Patrick, *ACS Nano* **2014**, *8*, 3461.

[13] a) M. G. Debije, P. P. C. Verbunt, *Adv. Energy Mater.* **2012**, *2*, 12; b) F. Meinardi, F. Bruni, S. Brovelli, *Nat. Rev. Mater.* **2017**, *2*, 17072; c) L. Dhamo, F. Carulli, P. Nickl, K. D. Wegner, V.-D. Hodoroaba, C. Würth, S. Brovelli, U. Resch-Genger, *Adv. Opt. Mater.* **2021**, *9*, 2100587.

[14] I. Levchuk, C. Würth, F. Krause, A. Osvet, M. Batentschuk, U. Resch-Genger, C. Kolbeck, P. Herre, H. P. Steinrück, W. Peukert, C. J. Brabec, *Energy Environ. Sci.* **2016**, *9*, 1083.

[15] a) R. Zeng, T. Zhang, G. Dai, B. Zou, *J. Phys. Chem. C* **2011**, *115*, 3005; b) J. J. Li, Y. A. Wang, W. Guo, J. C. Keay, T. D. Mishima, M. B. Johnson, X. Peng, *J. Am. Chem. Soc.* **2003**, *125*, 12567.

[16] B. Huang, H. Yang, L. Zhang, Y. Yuan, Y. Cui, J. Zhang, *Nanoscale* **2018**, *10*, 18331.